CHAPTER 5

NUMERICAL MODELLING OF FPSRS

5.1 Overview

The present chapter discusses the numerical model of FPSRS to understand in depth physics of the path that solar beam rays follow after reflection from reflectors, that is not easily observable in experiments as mentioned in the previous chapter. This numerical model is crucial for accurately identifying their intersection points and the angle formed by the reflected ray with the normal to the plane, serving as key parameters for determining the next intersection. To gain detailed insights into the behaviour of each ray the discretized methodology is used. Based on this, the RTA is developed using mathematical and derived equations for solar radiation. Additionally, guidelines for grid refinement are provided with considering the space and time dependent parameters, to determine the optimum number of grids for improving the accuracy of the analysis.

5.2 Numerical model

The numerical model of a physical system helps to understand the complex mathematics behind the physical process. The presented numerical model of FPSRS is crucial for accurately identifying their intersection points and the angle formed by the reflected ray with the normal to the plane, serving as key parameters for determining the next intersection. The derived solar radiation equations used for understanding the rays' behaviour as discussed in Section 3.1 of Chapter 3. Besides, the intersection of ray and reflector the three-dimensional analytical equations are used as presented in Section 3.2.

However, the actual applicability of solar radiation and geometric analytical equations is very important, and this can be understood through the detailed numerical modelling of the FPSRS presented in Fig 5.1. It helps in understanding the steps used to compute the path of the ray. For a better understanding of the reflection of the ray, the different behaviours of the rays are represented by various colours of the lines within the Fig. 5.1. The points P1, P2, …, Pn are represented as the intersection points on the reflectors, and (x_0, y_0, z_0) is represented as the global or reference coordinate system, while (x, y, z) is represented as the local or geometric coordinate system. The global coordinate system is considered a fixed point in the computation, where all other references are computed. However, the local coordinate system changes its coordinates according to the ray's

movement into the system. The terms $\widehat{u_1}, \widehat{v_1}$ and $\widehat{z_1}$ represent the coefficients of the normal vector of the reflector R1.

The reflection process begins by considering a single solar beam ray as a straight line, intersecting the TIS designated as P1. Subsequently, the interaction between the ray and the reflector is determined through the RTA and it is depicted as P2. The normal to all reflectors are then ascertained and the angle between the incident rays with the pertinent normal to the plane is computed to anticipate the ray's subsequent trajectory. The ray's subsequent interaction with the reflector results in its path being recorded as P3. The ray continues its course, engaging in multiple such reflections until it ultimately reaches the BRS. An elaborate expression to represent the plane, line, θ and the intersection point of the line with the plane during traversal for a typical ray is also delineated in Fig. 5.1.

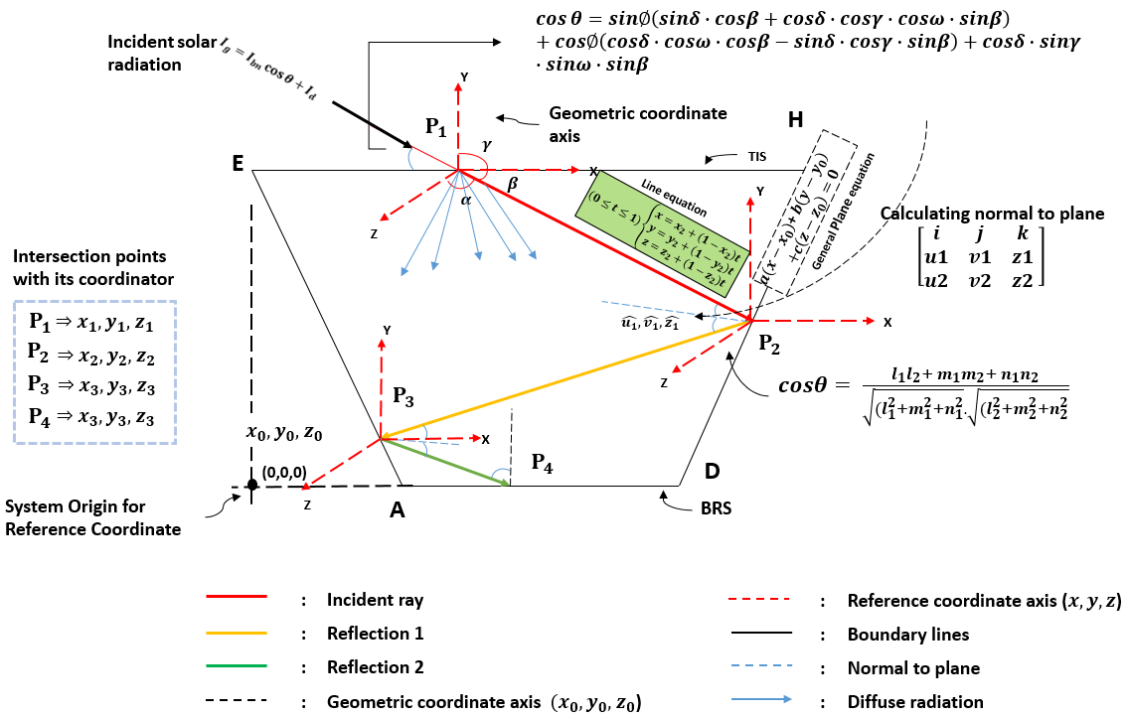

Fig. 5.1 Numerical modelling of the FPSRS

The discretized approach has been employed to illustrate the significance and contribution of each part of the FPSRS in the reflection process and the impact of rays on the receiving surfaces. To facilitate a better understanding, it is assumed that a ray passes through each small cell of the TIS. The discretization of the TIS into small cells and the core point through which the ray passes is illustrated in Fig. 5.2. It also provides an expanded view of the TIS, offering a clearer understanding of the location of all core points on it. The coordinates a1, a2, a3, and a4 represent the corners of a single cell on the TIS, with the respective core point being identified as n=1. The notations r1, r2, and r3,

along with c1, c2, and c3, denote the number of rows and columns, respectively, within the TIS in the discretization process. L1 and L2 are used to represent the two sides of the TIS. Furthermore, the marching direction of the core points on the TIS is depicted, providing a clear direction of steps to follow. This detailed visualization in Fig. 5.2 is crucial for the development of the RTA, which will be discussed in the subsequent section. The steps involved in the RTA, for which Fig. 5.2 plays a key role, are essential for a comprehensive understanding of the ray's path and its interactions within the system.

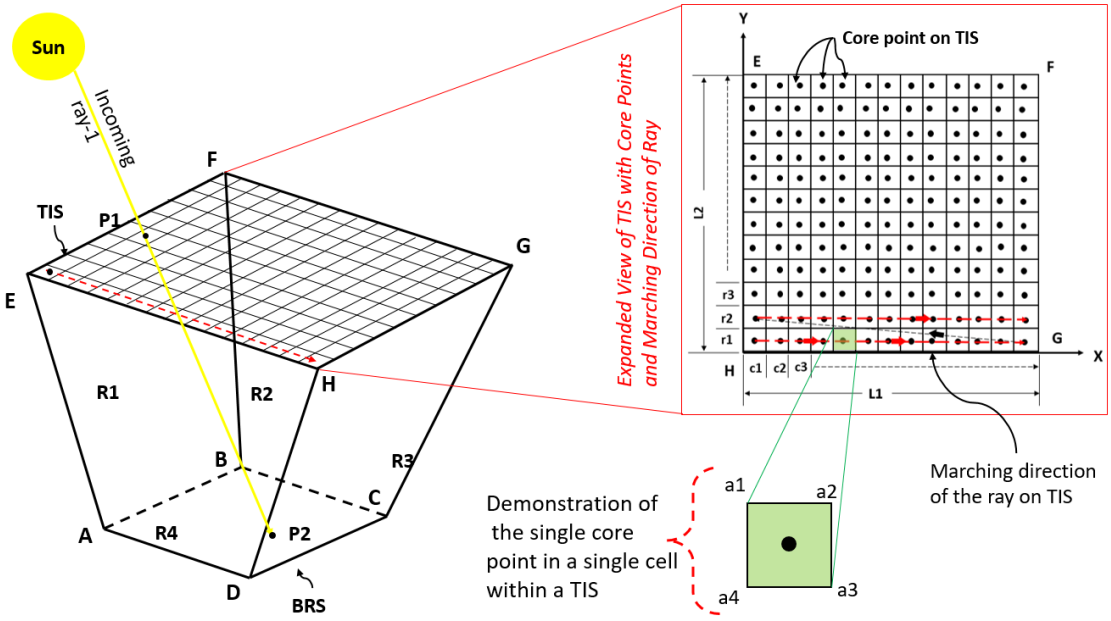

Fig. 5.2 Schematic representation of FPSRS with marching direction of ray on TIS.

5.3 Ray tracing algorithm

The behaviour of rays after reflection plays a vital role in deciphering the actual physics behind FPSRS and with the use of RTS it can be easily understand as detailed in Section 2.3. Several algorithms discussed in the open literature based on the RTS principle but these algorithms typically only provide information about a single reflection of a ray from a reflector and location on the receiving surface. However, they are unable to provide in depth detail like the path followed by rays after multiple reflections and the trajectory follow by the rays after it get interacting with neighbouring reflectors. Moreover, in real practical applications when dealing with complex geometries featuring multiple reflecting surfaces and rays undergoing multiple reflections before reaching the receiving surface, it is crucial for optical analysis. The 'Pucca cooker' (Apaolaza-Pagoaga et al., 2023) represents a geometry that can be better analysed optically if information about neighbouring reflections is available, along with all intersection points and the paths followed by the

rays. To address this limitation, the present section discusses the RTA. This significantly enhances the understanding of ray dynamics within FPSRS by explaining the unique way of handling the rays based on their number of reflections and their interaction with opposite and neighbouring reflectors.

Moreover, the integration of a discretized approach into the RTA has been a key factor in this enhancement, offering detailed insights into the localized effects of small areas of the reflector. This precision allows for accurate prediction of ray behaviours in complex systems and helps in optimizing design as well as efficiency of the system. The detailed RTA is depicted in Fig. 5.3. In the present study, three different types of configurations (STA, HTA, and OTC) have been discussed to compare their best optical performance of FPSRS. However, in current section, the RTA is discussed concerning the STC of FPSRS, while the optimized FPSRS considering HTC and OTC are discussed in the next chapter.

The RTA is developed and tested using MATLAB software. Initially, the computation begins by selecting the geometric data (STC or HTC or OTC) and entering the required input conditions for considering the basic configuration of FPSRS. Next, the line and plane functions are utilized to obtain the coordinate details of the geometry and to gather information on the line and plane equations of the selected configuration-based FPSRS. In this case STC has been selected and the total number of nodes is initialized to be greater than one to prevent inline errors on the TIS. The value of θ is constrained to range between 0° to 180°, considering the maximum possible movement of the sun over the earth. Once all input conditions are entered, the algorithm stores all reflecting plane equations, their coordinates, and the normal equations of each plane. Later on, all the data are stored by entering the input solar radiation condition, which in the present case is the Summer solstice (SS) and Winter solstice (WS).

The RTS then proceeds by considering each core point one-by-one in this process (refer to Fig. 5.2 for the incremental arrangement of core points). Subsequently, each ray begins to interact with the reflector and either reaches the BRS or exits the system through the TIS. Based on the number of reflections and the final possibility of remaining within the system or exiting it, the rays are categorized into their respective types, as outlined in Table 4.2. The algorithm continues by selecting the next core point from the TIS for simulation, and so on. This process continues until all the core points on the TIS have been passed through, and finally the algorithm is terminated. In the following section, the optimum number of grid points selected for the study is discussed, considering the time and space-dependent parameters and providing guidelines for a grid-independent study.

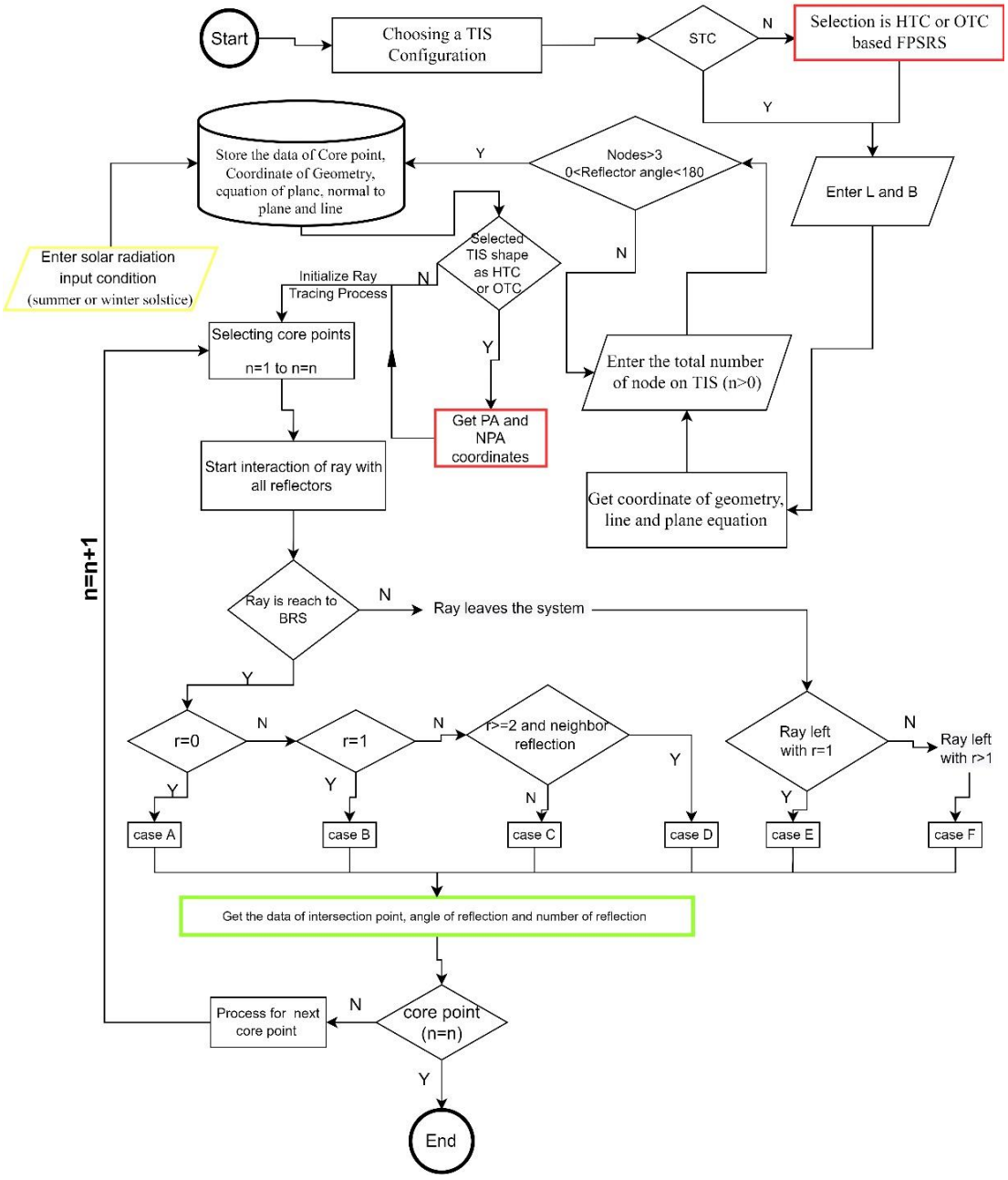

Fig. 5.3 Ray tracing algorithm for predicting the behaviour of solar ray.

5.4 Guidelines for grid refinement process

The significance of selecting an N for numerical computational problems and the deficiencies inherent in conventional methods have been discussed in section 2.6 for STS. The present section addresses this issue by providing a solution-oriented guideline for determining the N in complex FPTR enhanced solar computational problems. Through a case study featuring an FPSRS with STC, along with the utilization of a separate *'RTA for Grid refinement known as RTA-G'*, the proposed guidelines have been validated. The guideline comprises two steps: firstly, employing the LC and

EGR methods to swiftly identify regions requiring grid refinement. This approach significantly diminishes computation time for grid refinement by promptly identifying critical areas. The second stage involves determining the correct value of N using the CVRMSE and the R^2 approaches. Here, LC and EGR serve as *'indicative methods'*, while CVRMSE and R^2 function as *'deterministic methods'*. Sequencing the indicative approach followed by the deterministic method results in a notable reduction in the total refinement stages. In the following discussion the methods and guidelines discussed followed by the obtained results.

5.4.1 Methods used for grid refinement process

The basic information about the individual methods used for the grid refinement process is discussed in Section 2.6. However, the mathematical importance behind the used methods are discussed in the following discussion. Mainly, the methods can be classified into three categories: a) methods that are based on random sampling, b) methods that specify a limiting value rather than a specific number, and c) methods that help to find the specific value of N.

First, the SRS method is discussed as it mainly works on the principle of random sampling. The use of SRS method found very common in the literature and the method is based on random sampling. Under this every element in a population has an equal chance of being chosen for the sample. The Eqs. (5.1) to (5.3) (Q. Chen & Srebric, 2002) are being used to find out the sample getting selected (p), sample variance (σ) and population mean ($\bar{X}$) for these samples are obtained as mentioned below. Here, N_n is represent the total number of run taken for study and n is the sample size. The major advantage of adopting SRS is it works well in case of any grid number, even for coarse grid. This is because the SRS uses the number of grid points only. However, the SRS fails to give any statistical quantification of a definite value of possible error in the results obtained and so the use of it is discouraged (Pang et al., 2021).

$$p = 1 - (1 - \frac{1}{N_n})n \tag{5.1}$$

$$\sigma^2 = \frac{\sum_{i=1}^{N}(X_i - \bar{X})^2}{N_n} \tag{5.2}$$

$$\bar{X} = \frac{\sum_{i=1}^{N} X_i}{N_n} \tag{5.3}$$

There are certain methods that suggest a limiting value of grid refinement rather than an exact number of grid points, two such relevant methods are EGR and LC method. The EGR method uses the grid numbers between the two consecutive generations (N_1 and N_2) and size of grid (d or L) as an evaluating parameter. Here N_{n+1} and N_{n+2} represent the grid numbers and d, or L is the linear dimension of small element. With every increase in the number of grid point's value of EGR

decreases. In an extreme case, value of EGR ≤ 1.1% (Pan et al., 2018). Any increase in the grid number beyond this point will bear no effect on EGR. This shows that the use of EGR itself will not give a numerical limiting value for choosing N, however, its implementation gives a necessary condition for choice of N for a grid independent solution. The mathematical description of EGR is as shown in Eq. (5.4) (Pan et al., 2018), while the ratio of two successive grid numbers is defined by normal grid reduction ratio (NGRR) which can be obtained from Eq. (5.5) (Hatami & Walsh, 2023). Another such methods in this category are LC method. The method helps in defining the scale of a physical system. It is represented by the ratio of 'grid resolution (R)' and the 'max of dx or dy (W)' as shown in Eq. (5.6). Where, the R is the distance between the nodes on the grid and W is the corresponding length of the measured resolution. Recommended value of LC for optimum grid resolution range is less than 3% (Lee et al., 2020b). Like EGR method, the LC method also recommend a range to follow and do not provide an exact value of N.

$$EGR = \left(\frac{N_{n+1}}{N_{n+2}}\right)^{(1/d)} \tag{5.4}$$

$$\text{NGRR} = \frac{N_{n+1}}{N_{n+2}} \tag{5.5}$$

$$LC = \frac{Grid\ Resolution}{\max of\ [dx\ or\ dy]} = \frac{R}{W} \tag{5.6}$$

There are certain methods in this category which suggest exact number of grid points, these are CVRMSE and the R2 method. The CVRMSE method is derived from the Root-mean-square error (RMSE) method. The implementation of RMSE helps in determining the N that gives absolute fit of the model and shows the closeness of the predicted values with that of the actual data points. The value of RMSE can be obtained from Eq. (5.7) (Masters et al., 2013) where, M_i represents the best achievable result considering an infinite grid number, while S_i is the result obtained considering a particular grid number. However, the CVRMSE is a slight modification to RMSE, in this, the method normalizes the equation by use of total number of grid cells as shown in Eq. (5.8). Literature suggested that for the value of CVRMSE (if found ≤ 5%) the improvement in predicted results with increase in the grid numbers will become a constant and the corresponding grid number will be optimum (Miyashita & Yamada, 2005).

$$RMSE = \sqrt{\frac{\sum_{i=1}^{N}(M_i - S_i)^2}{M_i}} \tag{5.7}$$

$$CVRMSE = \frac{1}{N_i}\sqrt{\frac{\sum_{i=1}^{N}(M_i - S_i)^2}{M_i}} \tag{5.8}$$

The R^2 method serves as a statistical measurement technique assessing the variance in outcomes of a specific event due to differences in each variable. Its primary utility lies in revealing the trends within obtained results. R^2 spans a range from 0 to 1, where 1.0 signifies a perfect fit, indicating a highly reliable model for future projections, while a value of 0 indicates a failure to adequately describe the data. The literature states that the variation between the expected and actual values stabilizes and indicates an ideal estimation of N when the R^2 value is 0.95 or higher. The mathematical representation of R^2 is provided in Eq. (5.9) (Serani et al., 2019). Subsequent discussions delve into the application of these methods.

$$R^2 = 1 - \frac{\sum_i (M_i - S_i)^2}{\sum_i (M_i - \bar{M}_i)^2} \tag{5.9}$$

5.4.2 Proposed guidelines for grid refinement process

Based on the above discussion it is stated that the LC and EGR methods will not give any specific value of grid number or any statistical quantity that can be implemented for an exact value of number of grids. However, these methods can be employed to quickly locate a region where refinement of grid number is critically wanted. In other words, the method significantly influences the process of refinement and reduces the number of iterations by quickly identifying the critical region for the improvement. The application of the LC and EGR methods, therefore, can be helpful in identifying or quickly spotting a zone of refinement. However, these methods itself cannot quantify the grid refinement, in terms of any the grid numbers. Therefore, these methods can best serve as an 'indicative method' and lay a necessary condition in the search of zone of refinement. Furthermore, since method helps in determining the GGI area within a given numerical model, it will help reduce the total execution time for arriving at optimum grid number N, and reduces overall time needed for subsequent grid optimization processes.

Other two methods, CVRMS and R^2 methods are methods that results into grid numbers. Both these processes are standalone and can lead to optimum value of N. However, the process of grid refinement is iterative one and takes large number of iterations to refine the grid. The process can be continued for reducing the error generated during the grid refinement process until a required grid quality is achieved. These methods are therefore considered as "deterministic methods". Table 5.1 summaries characteristics of different methods.

Table 5.1 Summary of different method based on its characteristic.

#	Method	Type	Outcome	Limitation
1.	SRS	Intuitive	Grid number	Not verifiable
2.	LC, EGR	Indicative	Limits or range	Saturates beyond a certain value

3.	CVRMSE, R^2	Deterministic	Optimum grid number	Time consuming, need large iterations

Looking to the diverse nature of both the methods (LC and EGR on one hand and CVRMSE and R^2 on other hand), it is recommended to use both the methods in a definite sequence 'one after another' for best result or least number of iterations of grid refinement. The process of the improvement in adequate grid numbers can be accelerated if the indicative methods are used primarily to spot the region of refinement, i.e. by applying either LC or EGR method first. Since the implementation of LC or EGR helps in quickly point towards the location of a critical zone, where actual grid refinement will begin. As a second step deterministic method, i.e. CVRMS or R^2 method can be employed for grid refinement in the identified zone. The advantage of the sequential implementation of the indicative method followed by the deterministic method lies in the fact that the total number of refinement steps would reduce considerably. To assess the effectiveness of the proposed guidelines, the value of N is compared through a grid refinement process, calculated simultaneously using both Conventional methods (CM) and Proposed methods (PM), as illustrated in Fig. 5.4. Both the methods (CM and PM) have been demonstrated across two phases. In the first phase, the resulting grid number is selected. However, in the subsequent phase, input parameters are modified according to space- and time-dependent factors, and the resulting best grid size is obtained and analysed for best possible results.

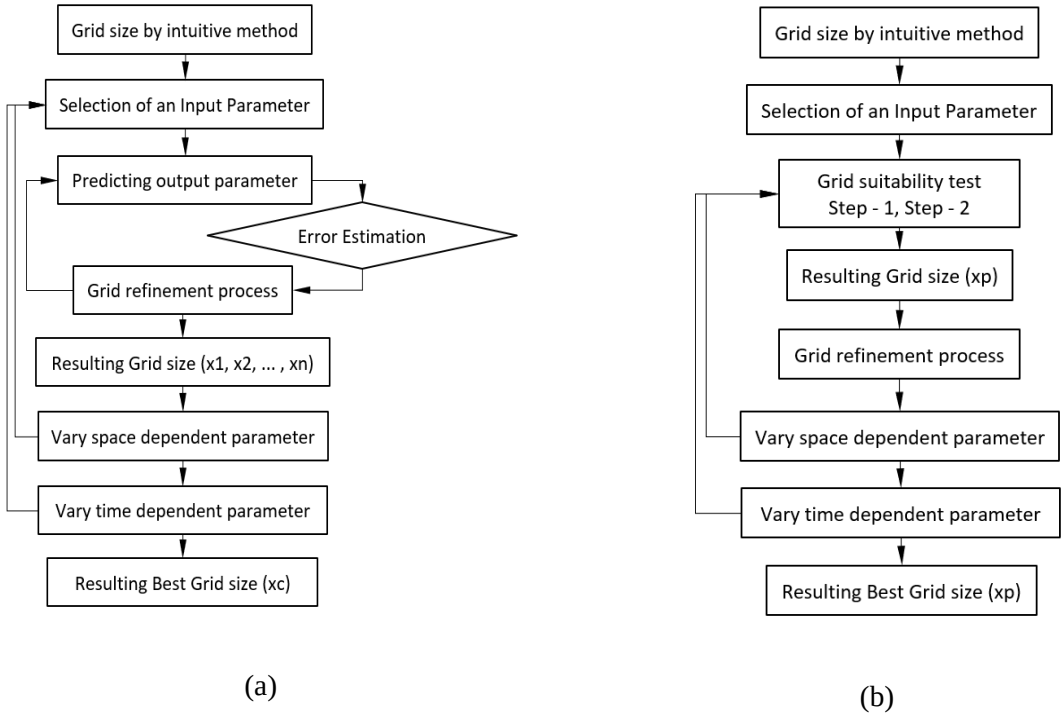

Fig. 5.4 Grid suitability test for a) CM and (b) PM.

In first phase, as depicted in Fig. 5.4 (a), within the CM, the grid size is initially determined using the SRS methods or an intuitive approach. Input parameters are selected, and the corresponding output parameters are recorded for subsequent modifications to the grid size. Through trial-and-error in the grid refinement process, the resulting grid sizes (x1, x2… xn) are obtained. In second phase, after incorporating space-dependent and time-dependent input parameters, the grid sizes vary. Consequently, the optimal grid size (xc) in CM changes with each alteration in space and time parameters. Conversely, in the PM, as shown in Fig. 5.4 (b), the resulting grid size (xp) is determined in first phase. In second phase, after applying space and time parameters, the optimal grid size remains consistent with the size obtained previously. The detailed steps to implement the PM for the FPSRS are outlined in Table 5.2 to enhance understanding.

Table 5.2 Description of PM for FPSRS

#.	**Descriptions**
i.	Chose a targeted geometry and decide input parameters.
ii.	Chose a targeted geometry and decide input parameters.
iii.	Prepare a list of different parametric combinations of various input parameters.
iv.	Identify the location of grid zone by applying indicative method i.e. LC or EGR method *(Step – 1).*
v.	Follow the corresponding identifying criteria of the method, i.e. EGR ≤ 1.1% or LC ≤ 3%.
vi.	Apply deterministic method and start actual grid refinement process.
vii.	Follow the corresponding refinement criteria for the grid refinement, i.e. CVRMSE ≤ 5% or $R^2 \geq 95\%$ *(Step – 2).*
viii.	Declare the obtained value of N.

5.4.3 Implementation of proposed guidelines for FPSRS having STC

Present discuss the application of the proposed two-step guidelines for determining the value of N in FPSRS equipped with STC. A distinct RTA, incorporating the proposed grid refinement methods and named 'RTA-G,' is developed to obtain the value of N for FPSRS. The RTA-G utilizes the same numerical model of FPSRS as discussed in Fig. 5.1, and employs a similar discretized approach and marching direction for the core points on the TIS, as illustrated in Fig. 5.2. However, the RTA-G distinguishes itself from RTA primarily in the selection method for the discretized number of cells on TIS, based on space and time. The methods used for discretizing the TIS is based on the space and time-dependent parameters. Initially, the grid points for the space system are denoted as ‘N1’. Then, considering different time instances throughout the day, a meshing scheme (N2 grid

points) for the transient coordinate is developed as a second step. This involves selecting the correct number of grid points N (N1*N2) for comprehensive analysis of the ray, aiming to deduce the energy intensity and its distribution at the base.

Initially, as a part of first step, the TIS is divided into fewer segments (say 5) herein referred as N1, and gradually increasing this until the best results are obtained, i.e. the results showing no significant variation with further increment in N1. Similarly, as a part of second step, fewer instances of sun position is considered (say 7) herein referred as N2 as summarised in Fig. 5.5 and Table 5.3. The labelling scheme for five distinct points on the TIS are i_{-2}, i_{-1}, i_0, i_{+1}, i_{+2} as illustrated in Fig. 5.5 and the labelling scheme for seven sun positions ranging from θ = 30° to 90° are j_{-3}, j_{-2}, j_{-1}, j_0, j_{+1}, j_{+2}, j_{+3} etc. Additionally, a quantity i_{avg} is obtained which is an average of these five points, which is used to infer the behaviour of a ray. As a first attempt the analysis considers a total of N1*N2 (36) divisions of the TIS, progressively the value of N1 and N2 can be increased after each iteration until the optimal grid size N is determined. For easy identification each test run is associated with a specific tag number. The calculations in the present analysis revealed that a total of 42 combinations were tested for the value of N as 2000. This amount to 84,000 number of tests performed by the algorithm.

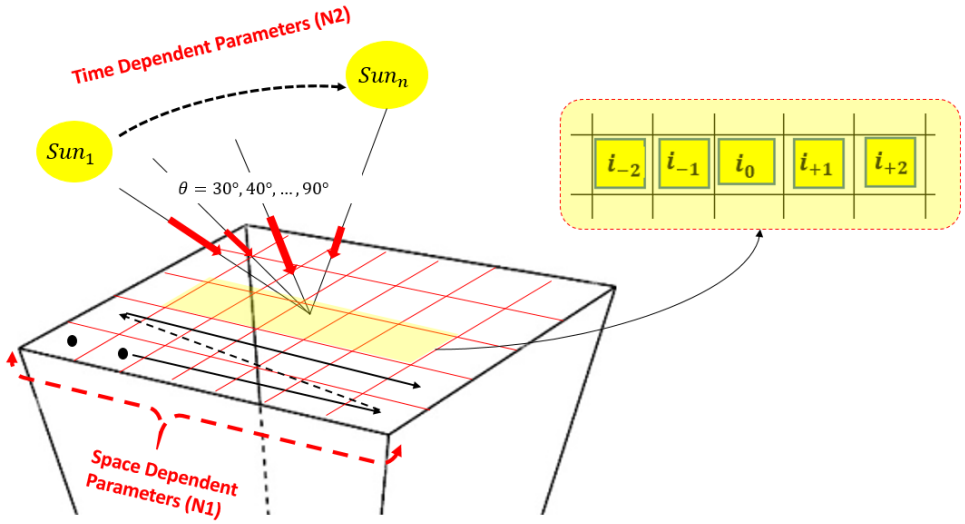

Fig. 5.5 Representation of space dependent parameters (N1) and time-dependent parameters (N2) to obtained N for FPSRS.

Table 5.3 Different positions of grid at different instances of ray

Cases	Angle & its Tag (N2)						
Position & its Tag (N1)	**(30°), j_{-3}**	**(40°), j_{-2}**	**(50°), j_{-1}**	**(60°), j_0**	**(70°), j_{+1}**	**(80°), j_{+2}**	**(90°), j_{+3}**

(i_{-2}), A	A1	A2	A3	A4	A5	A6	A7
(i_{-1}), B	B1	B2	B3	B4	B5	B6	B7
(i_0), C	C1	C2	C3	C4	C5	C6	C7
(i_{+1}), D	D1	D2	D3	D4	D5	D6	D7
(i_{+2}), E	E1	E2	E3	E4	E5	E6	E7
(i_{avg}),* F	F1	F2	F3	F4	F5	F6	F7

Note: * Position F corresponds to average of all the values of position A to E.

The analysis is started with considering single ray passing from TIS and its final available intensity at the BRS after multiple reflections. The schematic representation of the marching direction of the multiple rays is shown in the Fig. 5.2. However, the impact of time and space dependent parameters is shows in Fig. 5.5. Similarly, the total value of solar radiation on the TIS (I_{TIS}) and after reflection received radiation on the BRS (I_{BRS}) throughout the day is computed. To obtain this, several runs of the RTA-G are considered for different instances of space as well as time. Additionally, several assumptions (Patel, Jay, 2023; J. Patel et al., 2023) are made to simplify computations which includes (a) the reflector's symmetric geometry and its alignment with the sun's azimuthal position throughout the day, (b) considering a variation in θ between 30° to 90° due to minimal radiation intensity from 0° to 20°, (c) a consistent trajectory for the sun beyond 90° and (d) ray is passing from core point of the small area of TIS. Furthermore, upon examining the intervals between N2 grid points, it was observed that angles of 3° and 5° had no discernible effect on the final results when determining the value of N. These angles did not significantly impact the outcomes. Consequently, a decision was made to use 10° intervals in N2 as they appeared unaffected by changes in finer angles, ensuring stability in the final results. Operation of RTA-G with methods used for obtaining the N is discussed hereunder and is as shows in Fig. 5.6 and Table 5.4 shows the solar radiation data used for the study.

Table 5.4 Solar radiation data for Vadodara, Gujarat, India (April 2020) (*Solcast*, 2020)

$\theta°$	$\alpha_a{}^o$	T_{amb} (℃)	DHI (W/m^2)	DNI (W/m^2)	GHI (W/m^2)	$\gamma_z{}^o$
30	-103	33.9	149	250	189	63
40	-116	36.1	261	409	412	54
50	-146	37.8	372	538	597	42
60	158	37.9	460	616	587	34
70	121	38.2	482	669	765	22
80	105	37.9	511	658	786	16
90	97	38.0	562	661	685	2

Initially at time(t)=0, algorithm is initialised by considering given default initial condition of solar intensity, incident angle to horizontal and inclined plane, time, and day for the consideration. It is assumed that every cell (discretised small area) on the top is represented by a core point of the cell, and it is considered that a single ray is passing through each of it. For each reflector surface a corresponding function for plane equation was solved to obtain; a) the equation of plane, b) coordinates of plane, and c) normal to the plane (refer Fig.5.6). The process of ray tracing starts for the first ray considering counter 'i' and 'j' set as 1 each, and the information of ray interaction of each surface as it travers is obtained and stored until the ray is either reaches at the bottom surface or it escapes out from the system from top surface. The process is repeated for each ray considered for the analysis (N1). After this counter 'j' is set as 2 and the process is repeated for each N1 again. Process is stopped once counter 'i' reaches N1 and 'j' reaches to a value of N2. For each case quantity i_{avg} is obtained to determine adequacy of the selection of Ni points.

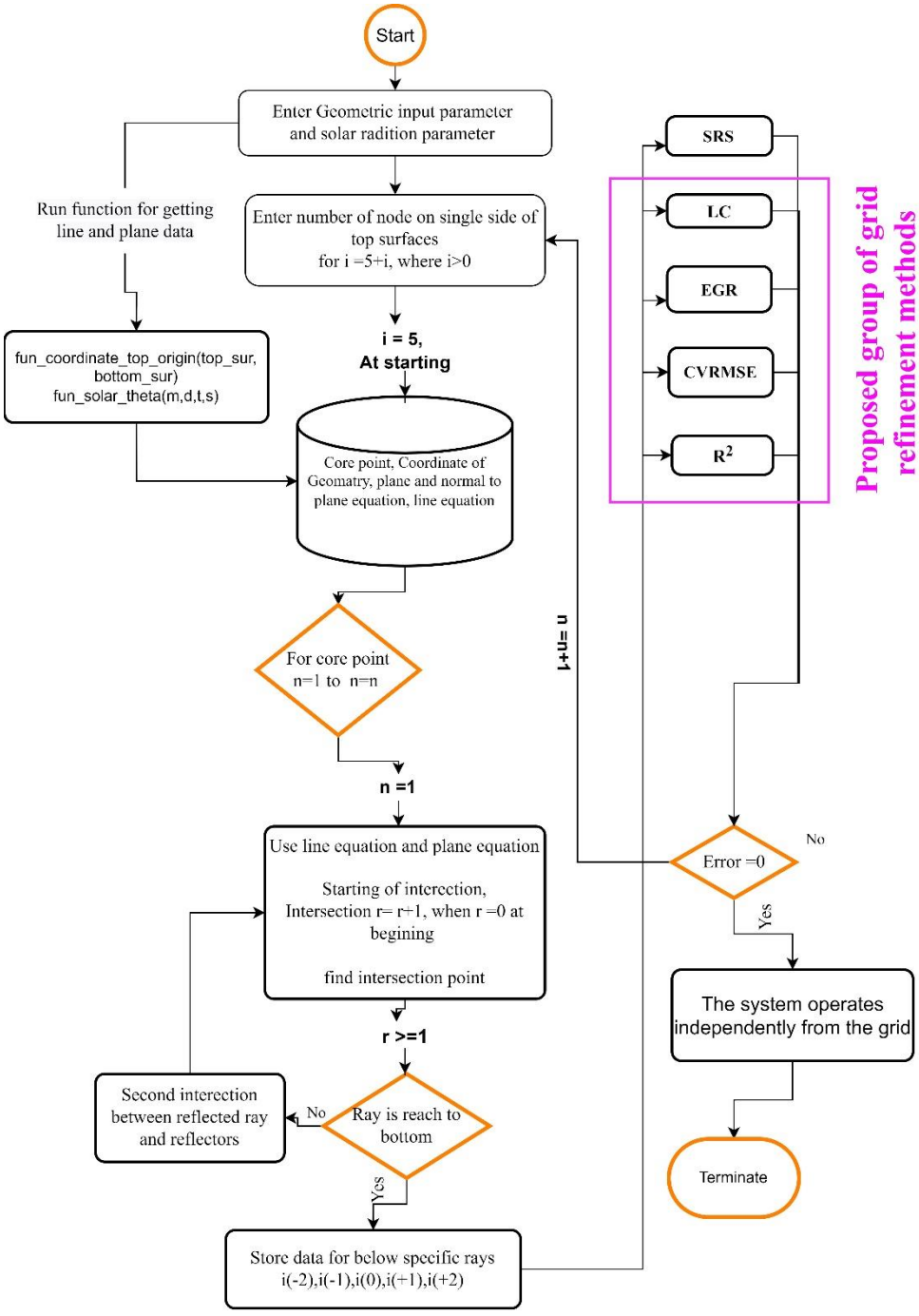

Fig. 5.6 The RTA-G used for FPSRS to predict the value of N for various situations.

5.4.4 Results and discussion

This section discusses the results obtained through CMs and PMs to determine the value of N for FPSRS. First, the results obtained from the CM are presented with highlighting the shortcomings or deficiencies present for obtaining the N for the FPSRS. Subsequently, a similar scenario of FPSRS

is considered and the results of the PM are presented to illustrate its applicability as outlined in the earlier section.

In CM, the value of N is typically selected based on intuitive methods or possibly SRS methods. Initially, the results of the intuitive methods used to select N are shown in Fig. 5.7 and Fig. 5.8. It is observed that with increasing the value of N step by step, the significant amount of reduction in the length of TIS cell (L_{Cell_TIS}) and similar for BRS cell (L_{Cell_BRS}) are found. The obtained results are shown in Fig. 5.7. It is also observed that the grid formation is coarse for the value of 0< N<500, fine grid for 500<N<1500, and very fine grid for 1500<N<2500. However, Fig. 5.8 represents the NGRR of the TIS, showing a reduction in the size of the two conservative cells on TIS. Literature suggests grid selection is typically done for the value of NGRR<1.2 (Hatami & Walsh, 2023). The probable selection range for N is highlighted in green and it is appears to be from 600 to 2500. As a consequence, while both results claim the region of the grid number, they do not claim the best grid number for the selected problem. Similar types of observations were made when SRS method was used to determine the ideal grid size; these observations are discussed in the section that follows.

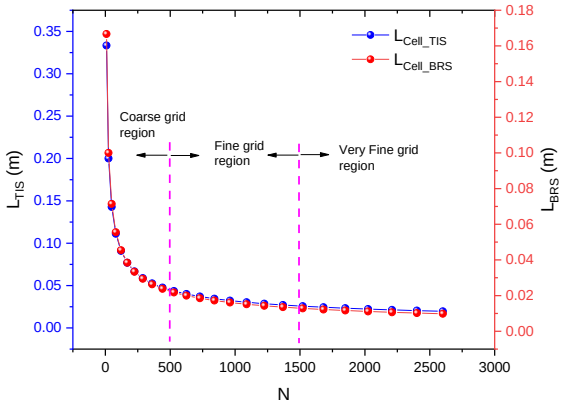

Fig. 5.7 Change in the grid size with increasing the value of N.

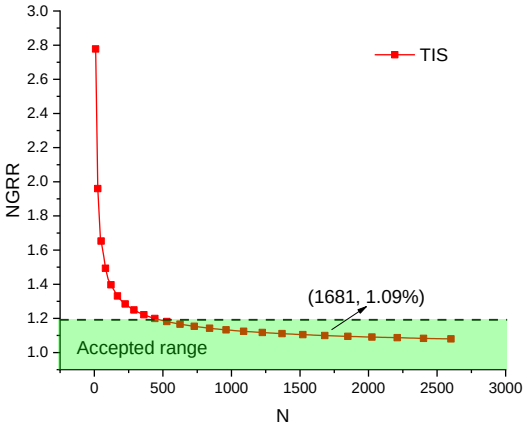

Fig. 5.8 Results of NGRR for TIS of the FPSRS.

The variation in I_{BRS} is illustrated in Fig. 5.9 while considering different grid numbers using CM for various cases as discussed in Table 4.2. For instant, Fig. 5.9 (a) depicts cases from A1 to F1 for Angle Tag (30°, 1) and the value of N is 1089. Whereas Fig. 5.9 (b) shows cases from A2 to F2 with an increased N value of 1225. Similar observations are made for other cases, where the value of N ranges from 1089 to 1681.Through these cases and spanning angle tags from 30° to 90° with different position tags, it's concluded that the CM implementation leads to uncertainty. Determining the N using the CM becomes challenging. This uncertainty results in a significant deviation, ranging from 6% to 13% over the mean value.

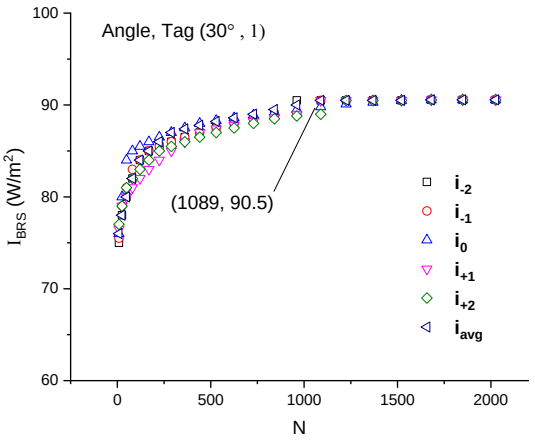
Angle, Tag (30° , 1)
(1089, 90.5)
I_{BRS} (W/m^2)
N
i_{-2}
i_{-1}
i_0
i_{+1}
i_{+2}
i_{avg}

(a)

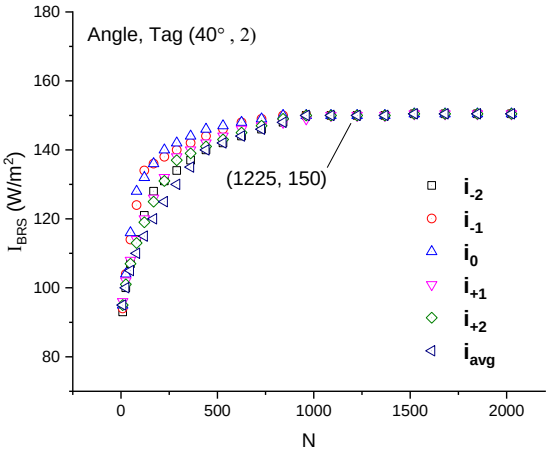
Angle, Tag (40° , 2)
(1225, 150)
I_{BRS} (W/m^2)
N
i_{-2}
i_{-1}
i_0
i_{+1}
i_{+2}
i_{avg}

(b)

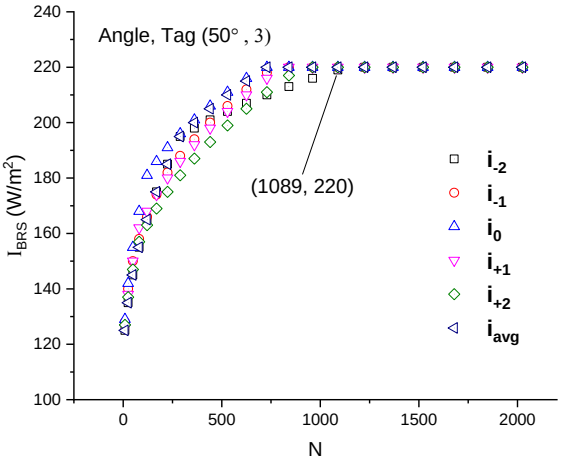
Angle, Tag (50° , 3)
(1089, 220)
I_{BRS} (W/m^2)
N
i_{-2}
i_{-1}
i_0
i_{+1}
i_{+2}
i_{avg}

(c)

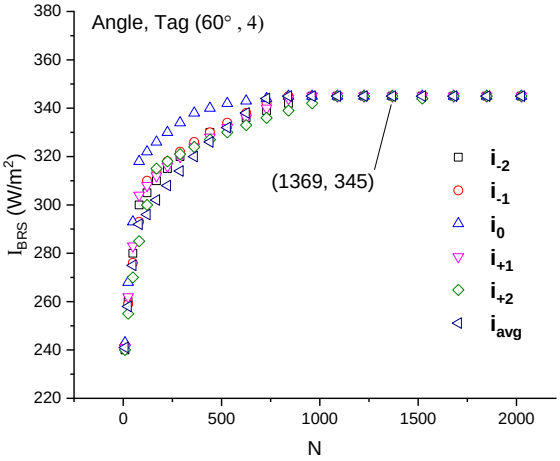
Angle, Tag (60° , 4)
(1369, 345)
I_{BRS} (W/m^2)
N
i_{-2}
i_{-1}
i_0
i_{+1}
i_{+2}
i_{avg}

(d)

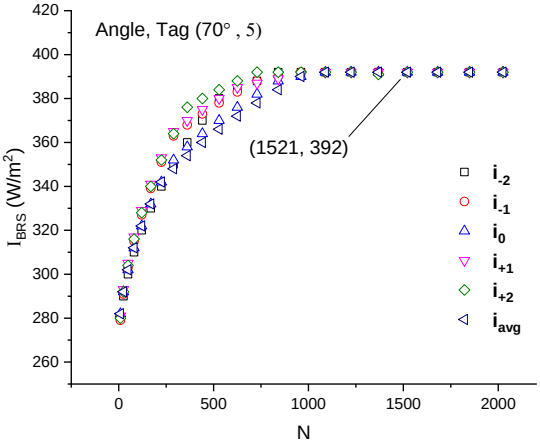
Angle, Tag (70° , 5)
(1521, 392)
I_{BRS} (W/m^2)
N
i_{-2}
i_{-1}
i_0
i_{+1}
i_{+2}
i_{avg}

(e)

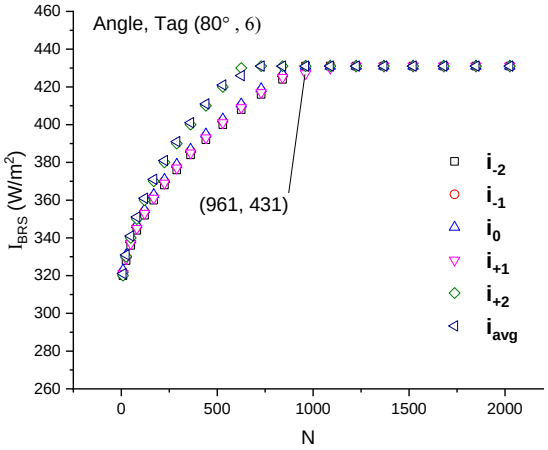
Angle, Tag (80° , 6)
(961, 431)
I_{BRS} (W/m^2)
N
i_{-2}
i_{-1}
i_0
i_{+1}
i_{+2}
i_{avg}

(f)

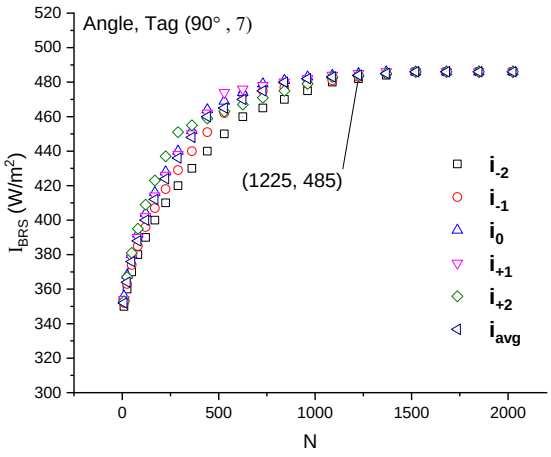

(g)

Fig. 5.9 Solar radiation received at BRS when N is selected with considering the CM.

Therefore, it is advisable to proceed with a parametric analysis to determine the ideal value of N. Initially, the refinement's critical zone was identified using the EGR or LC method, as detailed in in Section 5.3.2. The results obtained from the EGR method, aiding in pinpointing the critical region or GGI area for grid refinement across all 42 cases within the computational model is shown in Fig. 5.10. For the Angle, Tag (30°) the results are depicted in Fig. 5.10 (a) for cases A1 to F1, with similar trends visible in Figs. 5.10 (b) through Fig. 5.10 (g) for the other cases. Furthermore, literature indicates that an acceptable range for EGR is less than 1.1% (Lee et al., 2020b). However, from result it's observed that there's significant variation in EGR for the value of N from 0 to 450. There's a minor variation in EGR when N changes from 450 to 1100, and notably, minimal variation is observed after N reaches values from 1100 to 1521. Additionally, observations reveal a consistent trend of 'illusory convergence' across all cases while changing the values of N. The values of N within this zone of 'illusory convergence' exhibit significant variations across each case. Overall, it is discerned that the optimal value of N is not singular but falls within the range of 1225 to 1681 across these cases.

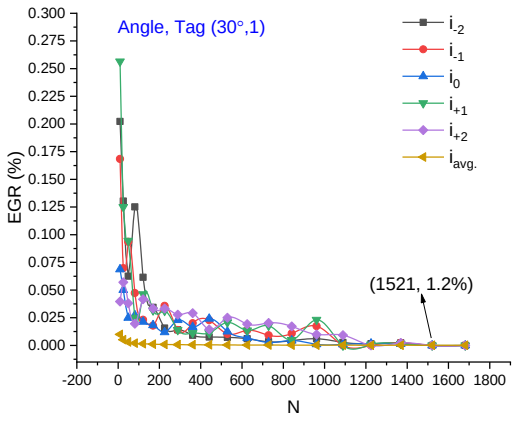

(a)

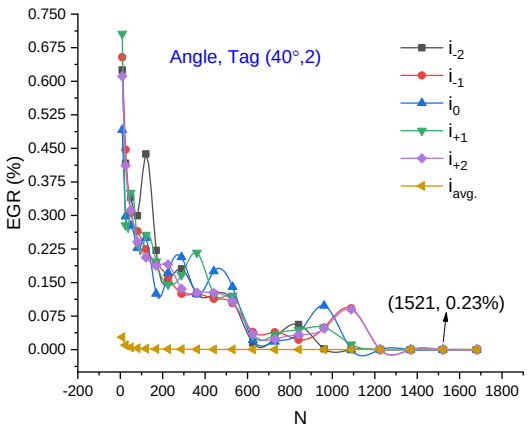

(b)

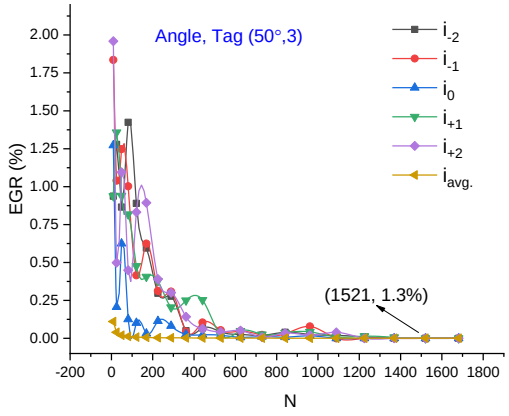

(c)

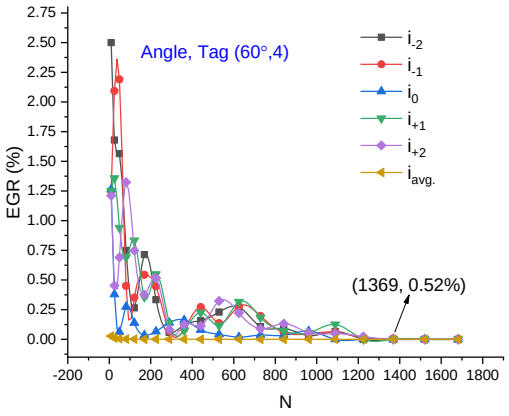

(d)

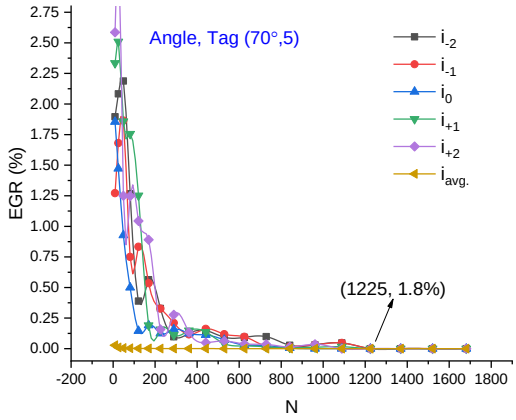

(e)

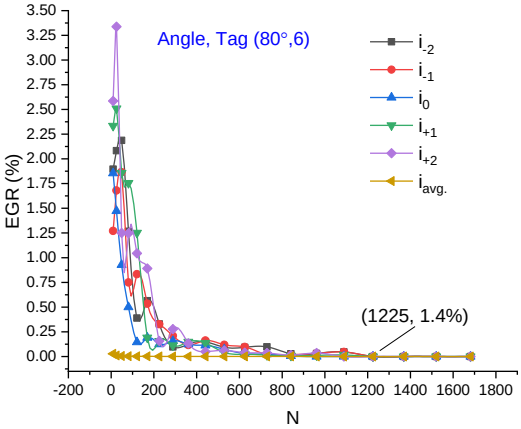

(f)

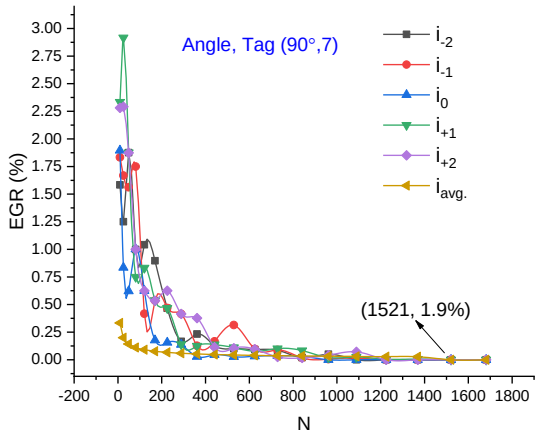

(g)

Fig. 5.10 Representation of critical zone with use of EGR.

The LC approach works well as a substitute for EGR in determining the GGI area inside the computational domain. When N is calculated using the LC approach, the results obtained for all cases are shown in Fig. 5.11. The literature indicates that when LC is less than 3%, the value of N is considered appropriate. Observations from the Fig. 5.11 reveal a significant variation in the LC value as N ranges from 0 to 500, followed by an exponential decrease between 500 and 1225. However, for variations in both angle tag and position tag, minor fluctuations are observed in the LC value when N

ranges from 1225 to 1681. Overall, from Fig. 5.11 (a) to Fig. 11 (g), it is evident that the acceptable range for N falls between 1369 to 1681 based on these observations. Nevertheless, it's crucial to recognize that a direct implementation of step 2 without completing step 1 isn't a prudent approach.

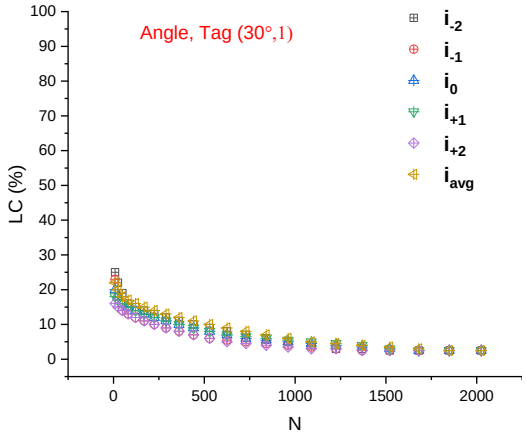

(a)

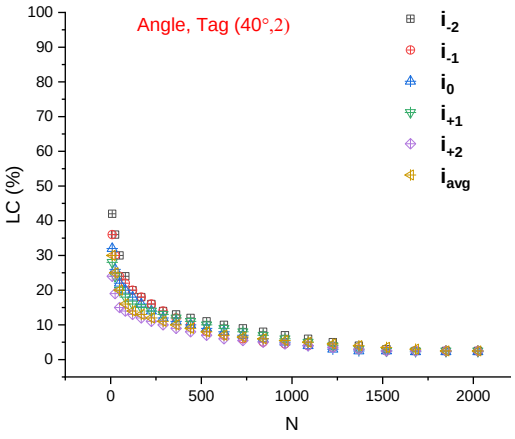

(b)

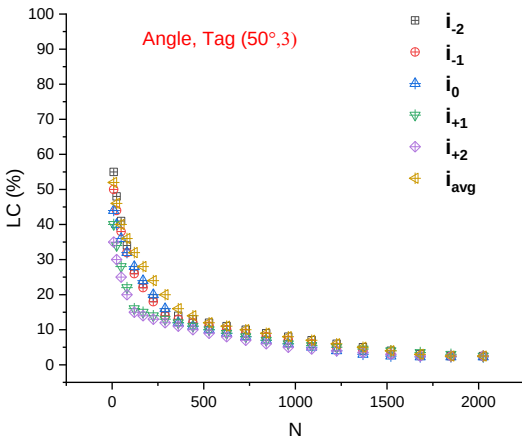

(c)

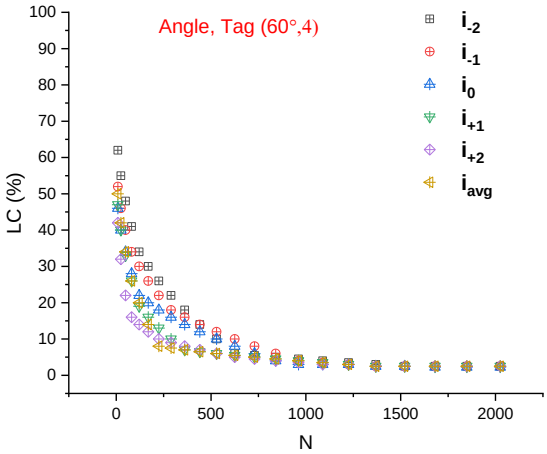

(d)

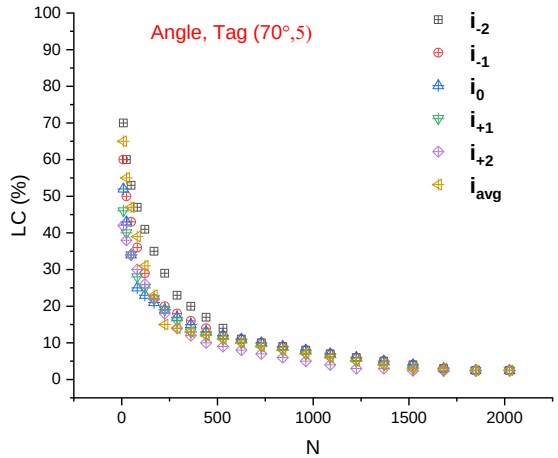

(e)

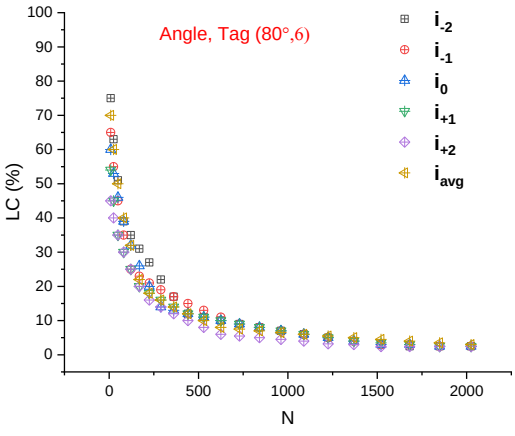

(f)

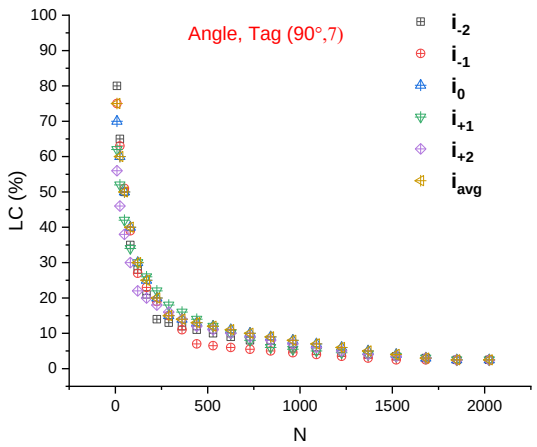

(g)

Fig. 5.11 Locating GGI region with help of LC method.

The obtained results after applying step 1 of PM, are discussed through the exponential view of the position tag of i_{avg} for EGR and LC methods, as shown in Fig. 5.12 (a) and Fig. 5.12 (b), respectively. The values of N is within the range of 1225 to 1861 while following the EGR condition. However, N is from 1396 to 1681 while following the LC condition. Overall, in comparison to CM, the values of N obtained from step 1 underscore the significance of both EGR and LC methods, highlighting the actual critical region where precise grid refinement becomes necessary.

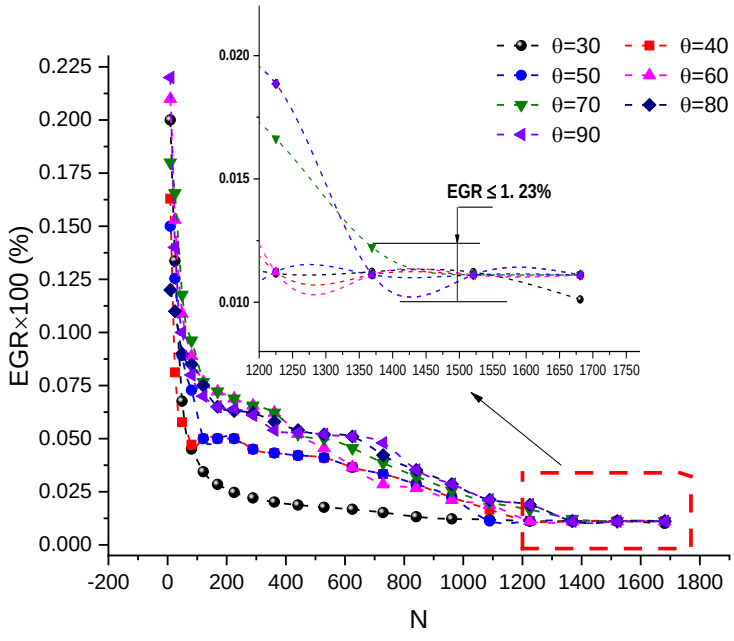

(a)

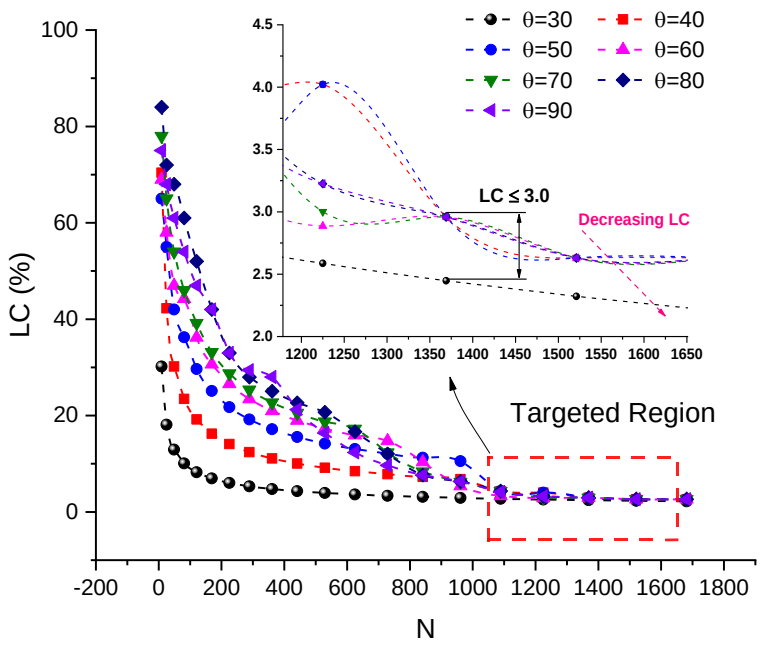

(b)

Fig. 5.12 Zone of '*illusive convergence*' using; (a) EGR method and (b) LC method (Exponential view).

In following the results obtained after applying the step 2 are shown. Step 1 helps in determine the GGI area of the computational domain however the unique value of the N can be obtained by applying CVRMSE or R^2 method as discussed in determination step of the guidelines. However, from step 1 is found that that the value of N is ranging from 1225 to 1681 and it is required to further investigate for finalised the final value of N. First, the results obtained from CVRMSE are presented in Fig. 5.13 for all the different cases when N changing 1225 to 1681. It will reduce the time of the overall computation as only certain range of N is only need to analyse. The results of CVRMSE for the similar angle tang has been shows from Fig. 5.13 (a) to Fig. 5.13 (g). From the literature it was found that the value of N is acceptable when CVRMSE is less than 5% (Miyashita & Yamada, 2005). It is also observed that the CVRMSE is about 10% for the angle tag is 30° and it reduce to 6% for the angle tag of 90°. It is represented that as the angle tag value increased there is sharp decline in the value of CVRMSE is observed and it lead to represent the stiffness in deciding the value of N. Besides this, there is huge variation is observed in the value of CVRMSE while N is changing from 1200 to 1500 and minor variation in CVRMSE when N is cross to 1500. However, there is no variation is observed when N value is reached to 1681. Finally from these study it is concluded that the final optimum value of N is 1681.

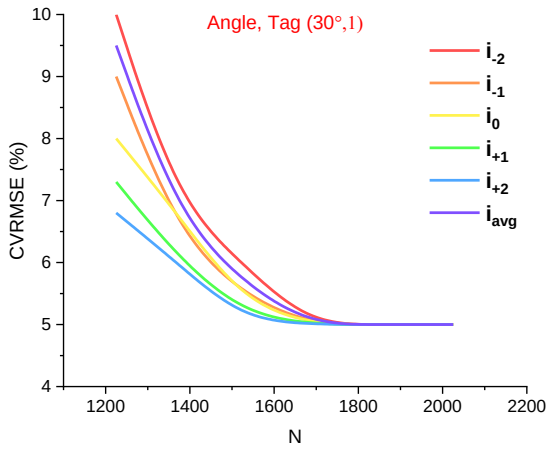
Angle, Tag (30°,1)
CVRMSE (%)
N
i_{-2}
i_{-1}
i_0
i_{+1}
i_{+2}
i_{avg}

(a)

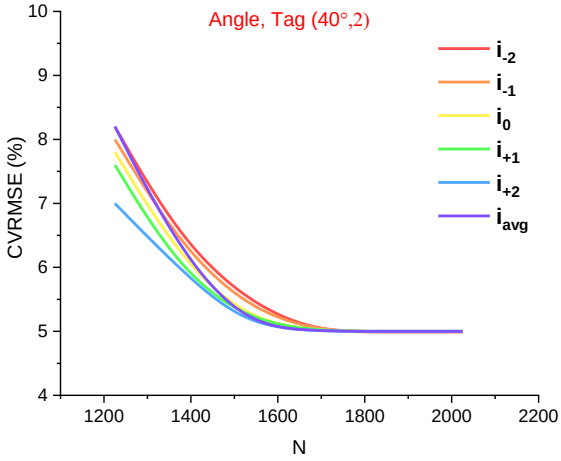
Angle, Tag (40°,2)
CVRMSE (%)
N
i_{-2}
i_{-1}
i_0
i_{+1}
i_{+2}
i_{avg}

(b)

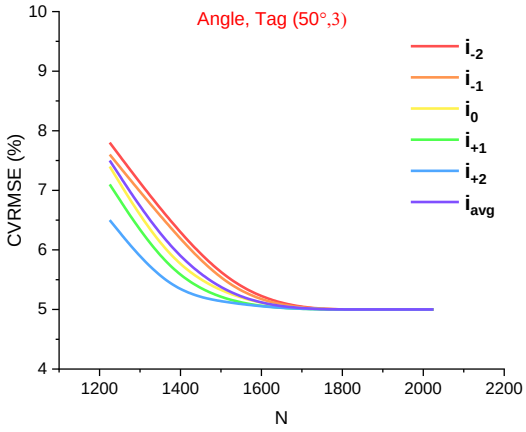
Angle, Tag (50°,3)
CVRMSE (%)
N
i_{-2}
i_{-1}
i_0
i_{+1}
i_{+2}
i_{avg}

(c)

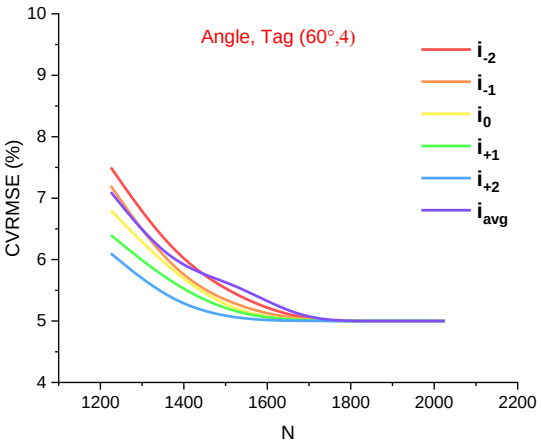
Angle, Tag (60°,4)
CVRMSE (%)
N
i_{-2}
i_{-1}
i_0
i_{+1}
i_{+2}
i_{avg}

(d)

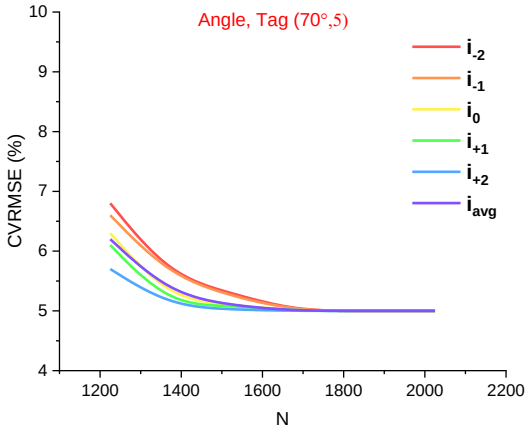
Angle, Tag (70°,5)
CVRMSE (%)
N
i_{-2}
i_{-1}
i_0
i_{+1}
i_{+2}
i_{avg}

(e)

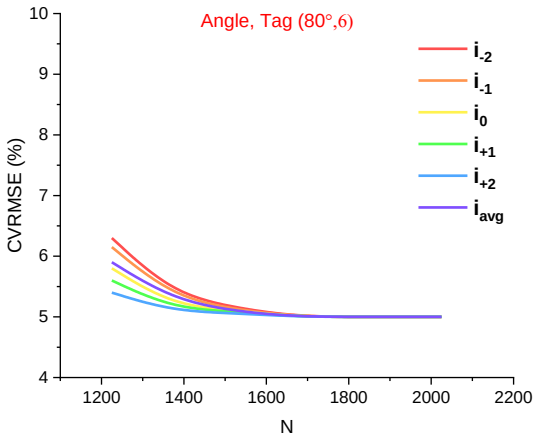
Angle, Tag (80°,6)
CVRMSE (%)
N
i_{-2}
i_{-1}
i_0
i_{+1}
i_{+2}
i_{avg}

(f)

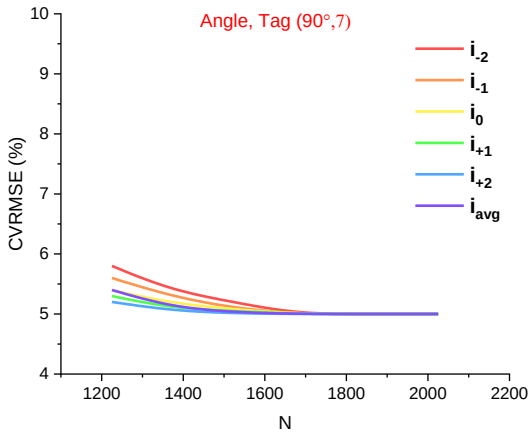

(g)

Fig. 5.13 Results of CVRMSE for obtaining the value of N.

While the R^2 approach can serve as an alternative to CVRMSE in determining the final value of N in step 2 where the initial step of the PM suggests that N should fall within the range of 1225 to 1681. The results derived from the R^2 method are presented in Fig. 5.14 and showcasing the observed response against the fitted response. Plotting the observed response involves the values of I_{BRS} for the predicted N value (I_{BRS_pre}) and the values of I_{BRS} for the actual N value (I_{BRS_act}). The actual value of N is Sequentially choosing from 1225, 1396, 1521, and 1681 and later it compared with the reference value of 1849 which is also known as the predicted value of N. However, the fitted response is deemed acceptable only when R^2 is less than 0.95. For instance, Fig. 5.14 (a) illustrates that the fitted response value is 0.73, which falls 0.22 points below the decided value of R^2 and it is necessitating further calculation. Similar outcomes are observed in Fig. 5.14 (b) and Fig. 5.14 (c). In contrast, Fig. 5.14 (d) demonstrates that the fitted response value is 0.95, meeting the acceptance criterion and requiring no further calculation. Thus, the chosen value of N in Fig. 5.14 (d) is considered as the final or the best value of N for the present FPSRS case study.

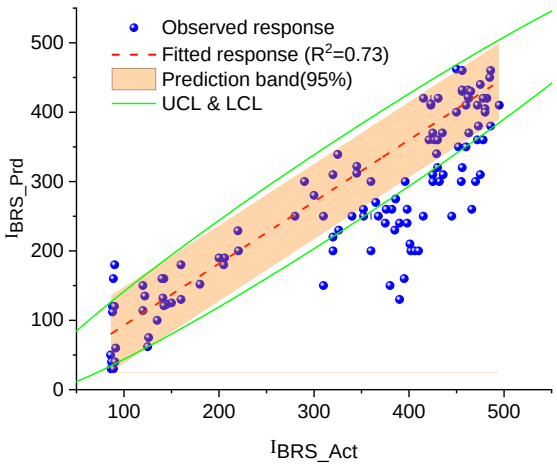

(a) N=1225

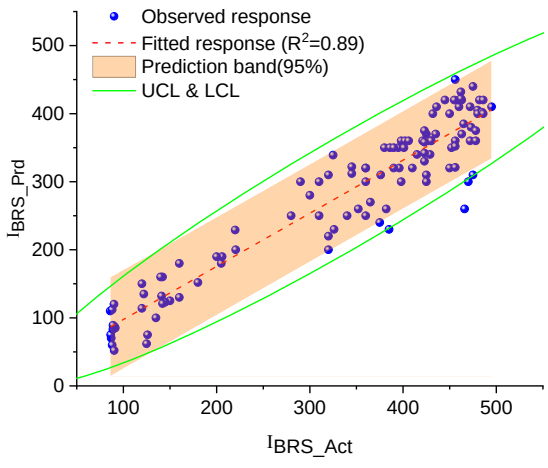

(b) N =1369

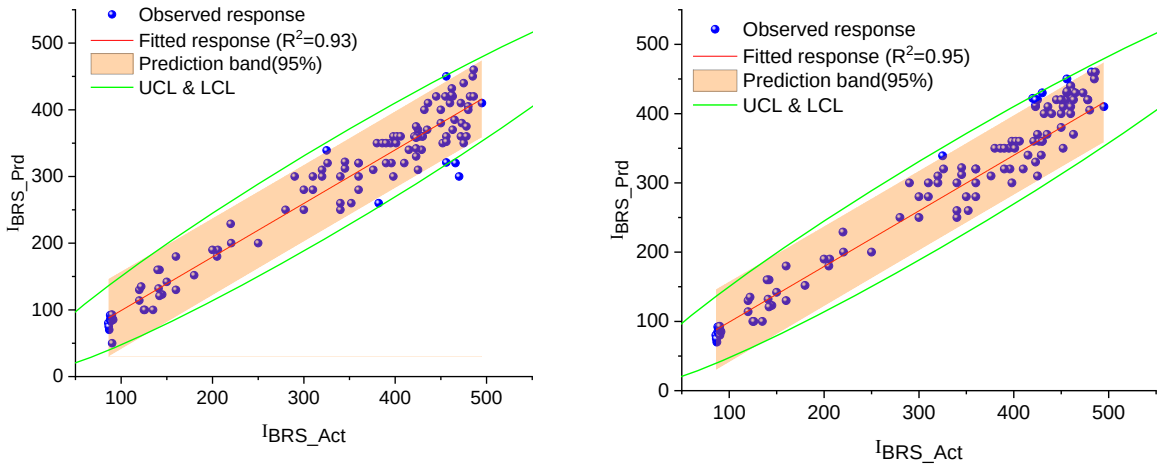

(c) N=1521 (d) N=1681

Fig. 5.14 Results of R^2 methods for finding the final value of N according to PM.

To obtain a single definitive value of N for all cases and arriving at a singular value proves to be quite challenging. Therefore, to showcase the actual impact of select critical cases on the selection of N, their results are presented here. Table 5.5 summarizes the results of N for specific critical cases (F1, F3, F7, A4, B4, and C4) after the implementation of step 2. It displays the final chosen value of N from both CM and PM. Additionally, a new metric named 'D' is introduced, defined as the percentage difference between the maximum and minimum values of N obtained for a specific set of observations. The results indicate that for CM, the overall value of ΔD stands at 4.3%. This disparity arises due to a significant variation in N, reaching 720, which is notably far from the desired accuracy and deemed unacceptable. Conversely, as predicted by PM, the final optimal grid number value of N is 1681, with a ΔD value of 0% across all cases.

Table 5.5 Comparative study of conventional and proposed method

Methods employed	Guidelines	Selection criteria	Measuring parameters	F1	F3	F7	A4	B4	C4	Observation
CM	No step	SRS	N	961	1089	1521	1369	1681	1521	ΔN = 720 &
			D	4.3	2.0	0.9	2.2	0.0	0.9	ΔD = 4.3%
PM	Step 1	EGR ≤ 1.1%	N	1225	1521	1681	1521	1369	1521	ΔN = 456 &
			D	2.7	0.9	0.0	0.9	2.2	0.9	ΔD = 2.7%
		LC ≤ 3%	N	1521	1681	1521	1521	1681	1681	ΔN = 160 &
			D	0.9	0.0	0.9	0.9	0.0	0.0	ΔD = 0.9%
	Step 2	CVRMSE ≤ 5%	N	1681	1681	1681	1681	1681	1681	ΔN = 00 &
			D	0.0	0.0	0.0	0.0	0.0	0.0	ΔD = 0%
		R2 ≥ 0.95	N	1681	1681	1681	1681	1681	1681	ΔN = 00 &
			D	0.0	0.0	0.0	0.0	0.0	0.0	ΔD = 0%

Overall, the developed two-step guidelines offer a systematic and scientific approach to determining the N for complex flat-type reflector enhanced solar computational problems. By leveraging the RTA in the context of a FPSRS, this study validates the efficacy of the proposed guidelines. Through a combination of indicative methods such as LC and EGR, followed by deterministic methods like CVRMSE and R^2, this approach not only streamlines grid refinement but also ensures greater accuracy in computational solutions. The sequential application of these methods significantly reduces computation time and enhances the accuracy of N determination. This systematic framework contributes to eliminating subjectivity in N selection, offering a robust and scientifically grounded methodology for future computational studies in solar energy systems.

Additionally, the importance of applying PM in traditional convergence solutions also helps in achieving better results. The process employed to achieve a converged solution, alongside a grid-free solution, is shown in Fig. 5.15. Traditionally, a converged solution follows a *'typical progression'*, denoted as the path a-b-c-d-e, which is widely adopted by most analysts and commercially available software. However, to ensure that the converged solution aligns with a grid-free solution, the current flow diagram can undergo modification, allowing for the proposition of a two-step method as shown in proposed guidelines. This proposed guidelines of grid refinement could potentially alter the process flow, introducing a modified path and denoted as a-b-c-f-g-d-e-h.

The implementation of this *'alternative methodology'* not only aims to ensure a grid-free solution but also strives to streamline the convergence time, presenting a more efficient approach to solution attainment. Moreover, the inclusion of a two-step method in grid refinement marks a significant advancement in computational techniques. It facilitates not only the attainment of a grid-free solution but also enhances the overall computational efficiency, thereby contributing to advancements in CFD and related fields. This innovative approach holds promise for improving accuracy while minimizing computational resources, thus benefiting diverse applications across various scientific and engineering domains.

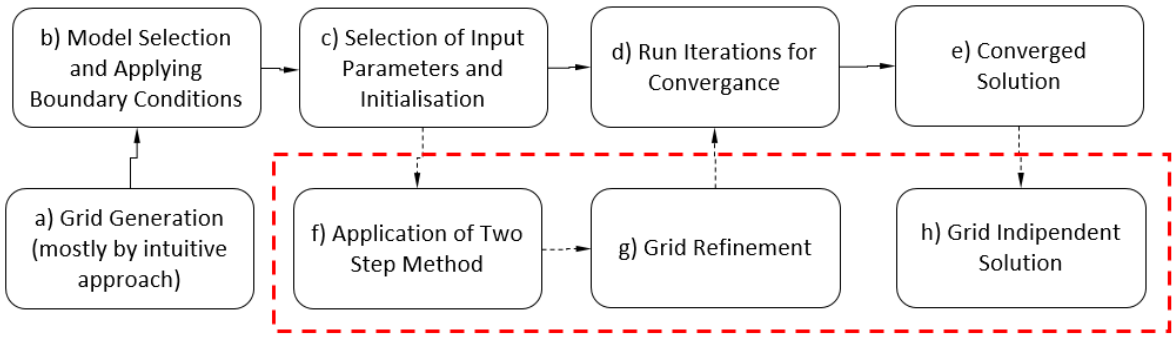

Fig. 5.15 Obtaining converged solution v/s grid free solution.

Looking forward, advancements in computational studies for solar energy systems can expand upon the proposed methodology. Future investigations might delve into integrating advanced machine learning techniques or optimization algorithms. These approaches could significantly enhance the efficiency of determining N. By incorporating AI-based algorithms or optimization strategies, the grid refinement and N selection process could become more automated and adaptable. Extending this framework beyond FPSRS to encompass a wider range of solar energy systems could yield comprehensive insights into various configurations. This expansion would enable a more generalized application of the guidelines. Moreover, as simulation tools and computing capabilities continue to evolve, there are opportunities to refine and expand this systematic framework. This evolution paves the way for increasingly accurate and efficient computational modelling in the realm of solar energy.

5.5 Summary

The present chapter helps in comprehending the numerical model of FPSRS, offering insight into the path followed by solar beam rays after reflection from reflectors with varying values of Φ. A gap identified in the experimental results reveals that information regarding neighbouring reflections from two adjacent reflectors can be more easily understood using the numerical model. This model is crucial for accurately identifying intersection points and the angle formed by the reflected ray with the normal to the plane, serving as key parameters for determining subsequent intersections. Utilizing unique discretized methods, the importance of each component's participation in the system is understood, emphasizing the significance of selecting the N for the discretized approach.

The choice of N significantly influences the accuracy of numerical solutions within discretized domains. To address the shortcomings of the CM method in calculating N, this work introduces a 'general-purpose two-step guideline' for its computation. Typically, researchers rely on past knowledge or the SRS approach for N selection, despite its potential for generating inaccurate results due to its simplicity. The first step in the proposed guidelines involves using EGR or LC techniques to identify grid areas requiring improvement. Subsequently, N is determined using R^2 or CVRMSE techniques. The article demonstrates the effectiveness of these guidelines through a case study featuring an FPSRS utilizing RTA. Additionally, it assesses the effects of changes in time- and space-dependent parameters. Moreover, important results from this investigation are also covered in brief in the section that follows,

1. The value of N obtained using CM with SRS techniques varies from 1225 to 1681, changing

due to variations in time and space variables, and it consumes a longer computation time. Conversely, PM swiftly identifies the GGI area initially for the chosen FPSRS case study and determines a final N value which is independent of time and space variables.

2. In step 1, EGR and LC show almost similar results for the present case study but might differ for others. In step 2, CVRMSE and R^2 yield similar N results, significantly reducing computation time compared to CM. However the final value of N obtain from the PM is 1681.
3. The efficacy of this approach demonstrates a remarkable 4.3% improvement in N determination compared to CM as seen from Table 5.5. These two-step guidelines, effective for FPSRSs, provide a systematic and scientifically grounded approach to N selection, eliminating subjectivity. Leveraging indicative techniques like LC and EGR, followed by deterministic methods like CVRMSE and R^2, streamlines grid refinement and enhances computational accuracy, significantly reducing computation time.
4. Looking ahead, future strides in computational studies for solar energy systems can build upon this groundwork. Integrating advanced machine learning or optimization algorithms holds promise to enhance N determination efficiency. Incorporating AI-based algorithms or optimization strategies can automate and adapt the process. Expanding this framework beyond FPSRS to encompass a wider range of solar energy systems could yield comprehensive insights into various configurations, allowing for a more generalized application of these guidelines.

Finally, as simulation tools and computing capabilities continue to evolve, there's ample scope to refine and expand this systematic framework. This evolution signifies a promising trajectory towards increasingly accurate and efficient computational modelling in the field of solar energy. Embracing advancements and continually enhancing methodologies in the quest for optimal N determination in solar computational problems can yield more accurate, efficient, and widely applicable solutions, thereby advancing solar energy research and applications.